

1     Scaling of collective flow of charged and identified  
2             hadrons in Au+Au collisions at  
3      $\sqrt{s_{NN}} = 11.5 - 62.4$  GeV from the STAR experiment

*Alexey Povarov (for the STAR Collaboration)<sup>a,1</sup>*

4             <sup>a</sup> National Research Nuclear University MEPhI,  
5             Kashirskoe highway 31, Moscow, 115409, Russia 1

6     Heavy-ion collisions create a hot and dense matter called Quark-Gluon Plasma (QGP). Azimuthal anisotropy of produced particles is sensitive to the transport properties of QGP (the equation of state, speed of sound and specific shear viscosity) and may provide information about initial state of the collision. In this work, we report results for elliptic ( $v_2$ ) and triangular ( $v_3$ ) flow of charged and identified hadrons ( $\pi^\pm, K^\pm, p, \bar{p}$ ) in Au+Au collisions at  $\sqrt{s_{NN}} = 11.5, 14.5, 19.6, 27, 39$  and 62.4 GeV from the STAR experiment at RHIC. Measurements of the collective flow coefficients  $v_2$  and  $v_3$  are presented as a function of particle transverse momentum ( $p_T$ ) and collision centrality. In addition the number of constituent quark scaling will be presented for these energies.

7  
8     PACS: 44.25.+f; 44.90.+c

9                             Introduction

10     One of the main goals of relativistic nuclear collision experiments is to  
11     study the properties of nuclear matter produced in heavy-ion collisions. In  
12     such collisions, extreme temperatures and energy densities are reached, which  
13     allows the creation of Quark-Gluon Plasma (QGP) where quarks and gluons  
14     are not anymore confined inside hadrons [1, 2]. First calculations of Lattice  
15     QCD indicated the transition from quark-gluon plasma to hadron gas [3].  
16     One of the main tasks of Beam Energy Scan program [4] at RHIC is the  
17     study of the QCD diagram in wide ranges of temperature T and baryon  
18     chemical potential  $\mu_B$ .

19     The azimuthal anisotropy of produced particles is one of the most widely  
20     studied observables. Azimuthal asymmetry in coordinate space in the col-  
21     lision of nuclei is created at the initial stages prior to the QGP evolution.  
22     Through the interaction of quarks and gluons, the azimuthal asymmetry  
23     in the coordinate space transforms into the anisotropy of the momentum  
24     space of the final products. It can be presented by the Fourier expansion of  
25     the produced particles azimuthal distribution relative to the reaction plane:  
26      $dN/d\phi \approx 1 + \sum_{n=1} 2v_n \cos(n(\phi - \Psi_n))$ , where n - order of harmonic flow,  $\phi$   
27     - azimuthal angle of particle and  $\Psi_n$  is the azimuthal angle of the n<sup>th</sup>-order  
28     event plane [5, 6]. The coefficients  $v_n$  are called coefficients of the anisotropic

---

<sup>1</sup>E-mail: povarovas@gmail.com

29 flow and can be used to quantitatively describe the azimuthal anisotropy.  
 30 The  $n^{\text{th}}$ -order flow coefficients can be calculated as  $v_n = \langle \cos[n(\phi - \Psi_n)] \rangle$ ,  
 31 where averaging is performed over all particles and events. Measurement of  
 32 the anisotropic flow allows to get information about the equation of state  
 33 (EOS) and transport properties of the strongly interacting matter [7, 8]. El-  
 34 liptic ( $v_2$ ) and triangular ( $v_3$ ) flow coefficients are the dominant signals and  
 35 have been studied at top RHIC and LHC energies [9, 10]. For the low  $p_T$   
 36 region ( $< 2 \text{ GeV}/c$ )  $v_2$  and  $v_3$  as a function of transverse momentum are  
 37 well described by viscous hydrodynamic models with small values of specific  
 38 shear viscosity  $\eta/s$  [11].

39 In this work we present new results of triangular flow for charged and  
 40 identified hadrons ( $\pi^\pm$ ,  $K^\pm$ ,  $p$ ,  $\bar{p}$ ) at midrapidity in Au+Au collisions at  
 41  $\sqrt{s_{NN}} = 11.5, 14.5, 19.6, 27, 39$  and  $62.4 \text{ GeV}$  from the STAR experiment at  
 42 RHIC and compare them to elliptic flow  $v_2$ .

#### 43 Data Analysis

44 The results presented in this work are obtained from the data by the  
 45 STAR experiment at RHIC. The data of Au+Au collisions at  $\sqrt{s_{NN}} = 11.5,$   
 46  $14.5, 19.6, 39, 62.4 \text{ GeV}$  used in this analysis are from the beam energy scan  
 47 program phase I and  $27 \text{ GeV}$  dataset is from the year 2018.

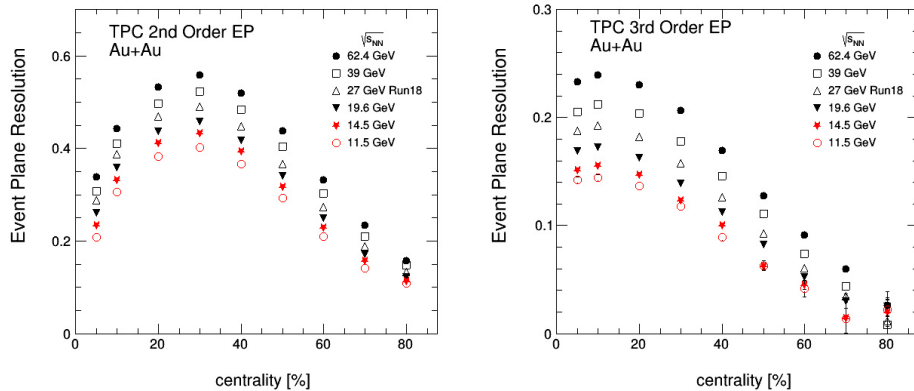


Fig. 1. The centrality dependence of the event plane resolution for  $v_2$  (left panel) and  $v_3$  (right panel) for six energies of collisions.

48 The selection of events was carried out using minimum bias trigger. Events  
 49 were selected with vertex position from the center of the detector along the  
 50 beam direction ( $V_Z$ ) of  $\pm 40 \text{ cm}$  for  $\sqrt{s_{NN}} = 39, 62.4 \text{ GeV}$ ,  $\pm 50 \text{ cm}$  for  $\sqrt{s_{NN}} =$   
 51  $11.5 \text{ GeV}$  and  $\pm 70 \text{ cm}$  for other energies. In addition the event vertex coordi-  
 52 nates in transverse plane ( $V_r = \sqrt{V_X^2 + V_Y^2}$ ) from the center of the beam  
 53 position were required to be less than  $1 \text{ cm}$  for  $14.5 \text{ GeV}$  and  $2 \text{ cm}$  for other  
 54 energies. Center of the beam position for  $14.5 \text{ GeV}$  was taken as  $(0.0, -0.89$   
 55  $\text{cm})$  due to shift in the beam along  $Y$  direction. In addition the number of  
 56 reconstructed tracks matching to the hits in TOF detector was required to be  
 57 more than 4 each events.

58 In this analysis primary tracks were used [12]. All tracks to have a min-  
 59 imum number of 15 fit points and the number of fit points is required to  
 60 be more than half (0.52) of the number of total possible points for track.  
 61 For charged hadrons, tracks were used with the distance of closest approach  
 62 (DCA) to the event vertex less than 2 cm and for identified particles less than  
 63 1 cm [12, 13]. All tracks are required to be within a pseudorapidity range  
 64  $|\eta| < 1$ . Information about charged particle ionization losses  $dE/dx$  in TPC  
 65 and  $m^2$  from TOF were used for the identification of  $\pi^\pm$ ,  $K^\pm$ ,  $p$  and  $\bar{p}$ .

66 In this work we used the event plane method for flow measurement [6].  
 67 Due to limited detector acceptance, recentering and flattening corrections  
 68 were applied to event plane angle [14]. Resolution of event plane was calcu-  
 69 lated by two sub-event method [15]. TPC tracks were divided into two part  
 70 (east  $\eta < 0$  and west  $\eta > 0$ ) and event planes were calculated in each sub-  
 71 event. We used  $\eta$ -gap ( $\Delta\eta$ ) between sub-events to reduce "nonflow" effect  
 72 such as decay of resonances, HBT correlation and jets. For charged hadrons  
 73  $\Delta\eta = 0.15$  and for identified particles 0.1. In Figure 1 resolutions of event  
 74 plane for  $v_2$  and  $v_3$  are presented as a function of collision centrality for six  
 75 energies.

## 76 Results

77 Results of  $v_2$  and  $v_3$  of charged hadrons as a function transverse momen-  
 78 tum  $p_T$  are shown on the left panel of Figure 2 for 5 bins of collision centrality:  
 79 0-10%, 10-20%, 20-30%, 30-40% and 40-60%. Values of triangular flow are

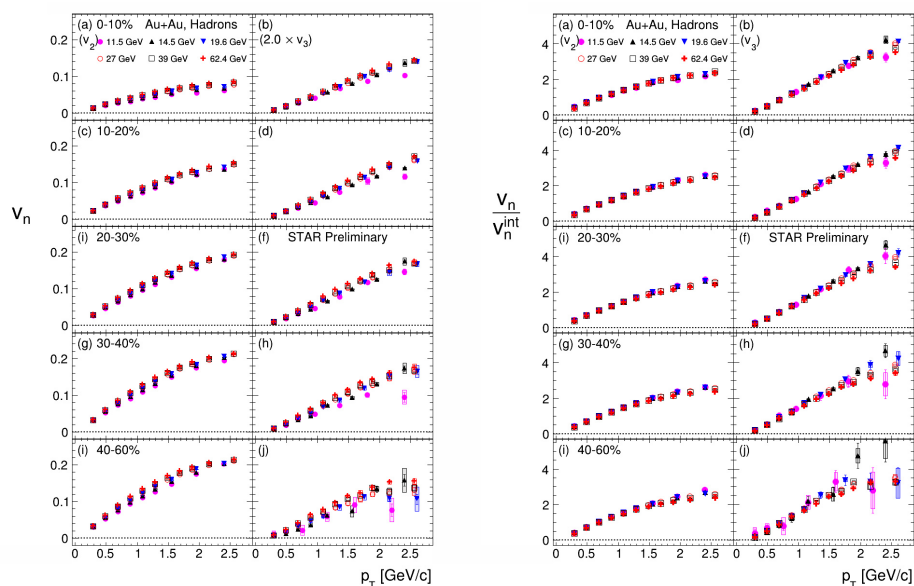


Fig. 2. Left:  $v_2$  and  $v_3$  of charged hadrons as a function of  $p_T$  for different collision energies and centrality. Right:  $p_T$ -dependence of  $v_2/v_2^{\text{int}}$  and  $v_3/v_3^{\text{int}}$  where  $v^{\text{int}}$  –  $p_T$ -integrated flow values.

80 multiplied by 2.0 for better comparison with elliptic flow. We see that

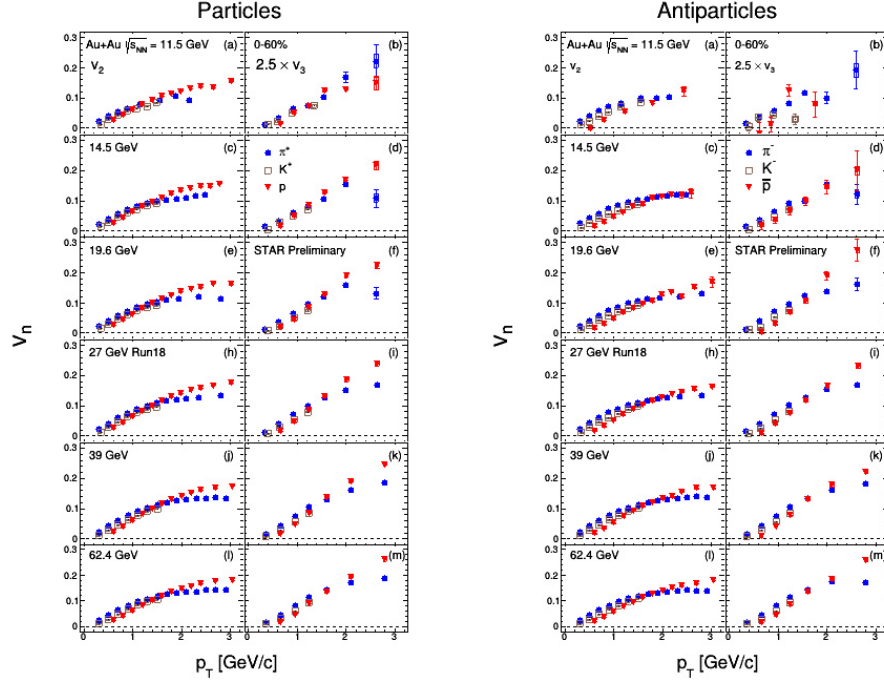


Fig. 3. Elliptic and triangular flow of  $\pi^+$ ,  $K^+$ ,  $p$  (left) and  $\pi^-$ ,  $K^-$ ,  $\bar{p}$  (right) for 0%-60% collisions centrality and six energies.

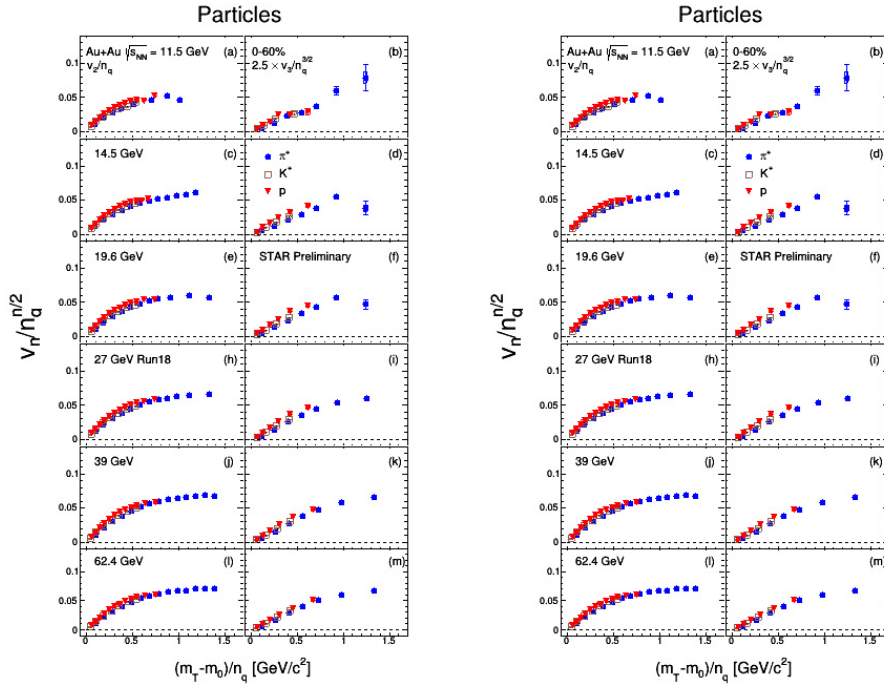


Fig. 4. The Number-of-Constituent Quark (NCQ) scaled  $v_2$  and  $v_3$  for 0%-60% central Au+Au collisions and six energies. Left panel - particles and right - corresponding antiparticles.

81 elliptic flow depends more on collision centrality than triangular flow. This  
 82 can be explained by the fact that  $v_2$  is more dependent on collision geometric  
 83 overlap of two nuclei whereas  $v_3$  is more dependent on initial density fluctu-  
 84 ations [16]. In the right panel of Figure 2  $p_T$ -dependence of  $v_n(p_T)/v_n^{\text{int}}$  is  
 85 presented where  $v_n^{\text{int}}$  is  $p_T$ -integrated  $v_n$  over  $p_T$  0.2 - 3.2 GeV/ $c$ .  $v(p_T)_n/v_n^{\text{int}}$   
 86 has a similar shapes for each collision centrality and energies, which is con-  
 87 sistent with theoretical predictions [17].

88 The  $\sqrt{s_{\text{NN}}}$  dependence of  $v_2(p_T)$  and  $v_3(p_T)$  for identified particles ( $\pi^\pm$ ,  
 89  $K^\pm$ ,  $p$ ,  $\bar{p}$ ) for 0-60% collision centrality are presented in Figure 3. The left  
 90 plot of this figure shows results for positive particles and the right shows  
 91 the same for negative particles. Values of triangular flow  $v_3$  are multiplied  
 92 by 2.5 to improve visibility. We see that triangular flow values have mass  
 93 ordering at low  $p_T$  range less than 1.5 GeV/ $c$  and meson/baryon splitting for  
 94 transverse momentum greater than 2 GeV/ $c$ . These effects were observed for  
 95  $v_2(p_T)$  in Au+Au collisions in previous measurements [18–21].

96 The number-of-constituent quark (NCQ) scaled  $v_2$  and  $v_3$  are presented  
 97 in Figure 4 as a function of  $(m_T - m_0)/n_q$  where  $m_T$  is transverse energy,  $m_0$   
 98 is particle mass and  $n_q$  is the number of constituent quarks. The left plot  
 99 shows results for positive particles and the right shows the same for negative  
 100 particles. Values of scaled  $v_3$  are multiplied by 2.5 to improve visibility.  
 101 Triangular flow of identified particles seems to follow the NCQ scaling. We  
 102 observed that values of collective flow for baryons and mesons lie on one  
 103 curve for each energy. This scaling holds better for higher energies. Values  
 104 of  $v_3$  for identified particles are new for this collision centrality and energies.

## 105 Summary

106 We have presented new measurements of triangular flow  $v_3$  with compar-  
 107 isson to  $v_2$  for charged and identified particles ( $\pi^\pm$ ,  $K^\pm$ ,  $p$ ,  $\bar{p}$ ) at midrapidity  
 108 in Au+Au collisions at  $\sqrt{s_{\text{NN}}} = 11.5, 14.5, 19.6, 27, 39$  and 62.4 GeV from  
 109 the STAR experiment at RHIC. Elliptic and triangular flow measurements  
 110 are presented as a function of  $p_T$  for different collision centrality and ener-  
 111 gies. Also the number-of-constituent quark scaling of  $v_2$  and  $v_3$  was shown.  
 112 We observed that  $v_3$  exhibits similar trends as for  $v_2$ . New values of  $v_3$  for  
 113 identified particles can serve as constraints for ultrarelativistic hydrodynamic  
 114 models.

## 115 Acknowledgments

116 The work was supported by the Ministry of Science and Higher Education  
 117 of the Russian Federation, Project “Fundamental properties of elementary  
 118 particles and cosmology” No 0723-2020-0041.

## REFERENCES

119

- 120 1. *Wilson K.G.* Confinement of quarks // Phys. Rev. D. — 1974. — V. 10. —  
121 P. 2445–2459.
- 122 2. *Shuryak E.V.* Quark-Gluon Plasma and Hadronic Production of Leptons,  
123 Photons and Psions // Phys. Lett. B. — 1978. — V. 78. — P. 150.
- 124 3. *Susskind L.* Lattice models of quark confinement at high temperature //  
125 Phys. Rev. D. — 1979. — V. 20. — P. 2610–2618.
- 126 4. *Aggarwal M.M. et al.* [STAR Collaboration] An Experimental Explo-  
127 ration of the QCD Phase Diagram: The Search for the Critical Point  
128 and the Onset of De-confinement. — 2010. — arXiv:1007.2613 [nucl-ex].
- 129 5. *Voloshin S., Zhang Y.* Flow study in relativistic nuclear collisions by  
130 Fourier expansion of azimuthal particle distributions // Zeitschrift for  
131 Physik C Particles and Fields. — 1996. — V. 70. — P. 665–671.
- 132 6. *Poskanzer A.M., Voloshin S.A.* Methods for analyzing anisotropic flow  
133 in relativistic nuclear collisions // Phys. Rev. C. — 1998. — V. 58, no. 3. —  
134 P. 1671–1678. — arXiv:9805001.
- 135 7. *Bernhard J.E., Moreland J.S., Bass S.A.* Bayesian estimation of the  
136 specific shear and bulk viscosity of quark-gluon plasma // Nature Phys. —  
137 2019. — V. 15, no. 11. — P. 1113–1117.
- 138 8. *Huovinen P., Petreczky P.* QCD Equation of State and Hadron Reso-  
139 nance Gas // Nucl. Phys. A. — 2010. — V. 837. — P. 26–53. —  
140 arXiv:0912.2541 [hep-ph].
- 141 9. *Adamczyk L. et al.* [STAR Collaboration] Azimuthal anisotropy in  
142 Cu+Au collisions at  $\sqrt{s_{NN}} = 200$  GeV // Phys. Rev. C. — 2018. — Jul. —  
143 V. 98. — P. 014915.
- 144 10. *Adam J. et al.* [ALICE Collaboration] Higher harmonic flow coefficients  
145 of identified hadrons in Pb-Pb collisions at  $\sqrt{s_{NN}} = 2.76$  TeV // JHEP. —  
146 2016. — V. 09. — P. 164. — arXiv:1606.06057.
- 147 11. *Gale C., Jeon S., Schenke B., Tribedy P., Venugopalan R.* Event-by-  
148 Event Anisotropic Flow in Heavy-ion Collisions from Combined Yang-  
149 Mills and Viscous Fluid Dynamics // Phys. Rev. Lett. — 2013. — V. 110. —  
150 P. 012302.
- 151 12. *Adamczyk L. et al.* [STAR Collaboration] Elliptic flow of identified  
152 hadrons in Au+Au collisions at sNN = 7.7–62.4 GeV // Phys. Rev. C. —  
153 2013. — V. 88, no. 1. — P. 014902. — arXiv:1301.2348 [nucl-ex].
- 154 13. *Adamczyk L. et al.* [STAR Collaboration] Inclusive charged hadron el-  
155 liptic flow in Au + Au collisions at  $\sqrt{s_{NN}} = 7.7 - 39$  GeV // Phys. Rev.  
156 C. — 2012. — V. 86. — P. 054908. — arXiv:1206.5528 [nucl-ex].

- 157 14. *Selyuzhenkov I., Voloshin S.* Effects of nonuniform acceptance in  
158 anisotropic flow measurements // *Phys. Rev. C.* — 2008. — V. 77, no. 3. —  
159 P. 034904. — arXiv:0707.4672 [nucl-th].
- 160 15. *Voloshin S.A., Poskanzer A.M., Snellings R.* Collective phenomena in  
161 non-central nuclear collisions // *Landolt-Bornstein.* — 2010. — V. 23. —  
162 P. 293–333. — arXiv:0809.2949 [nucl-ex].
- 163 16. *Alver B., Roland G.* Collision-geometry fluctuations and triangular flow  
164 in heavy-ion collisions // *Phys. Rev. C.* — 2010. — V. 81. — P. 054905. —  
165 arXiv:1003.0194 [nucl-th].
- 166 17. *Torrieri G.* Scaling of flow in heavy ion collisions and the low-energy  
167 frontier // *Eur. Phys. J. A.* — 2016. — V. 52, no. 8. — P. 249. —  
168 arXiv:1512.04704.
- 169 18. *Adler C. et al.* [STAR Collaboration] Azimuthal Anisotropy of  $K_s^0$  and  
170  $\Lambda + \Lambda^-$  Production at Midrapidity from Au+Au Collisions at sNN = 130  
171 GeV // *Phys. Rev. Lett.* — 2002. — V. 89. — P. 132301.
- 172 19. *Adams J. et al.* [STAR Collaboration] Multistrange Baryon Elliptic Flow  
173 in Au+Au Collisions at sNN = 200 GeV // *Phys. Rev. Lett.* — 2005. —  
174 V. 95. — P. 122301.
- 175 20. *Afanasyev S. et al.* [STAR Collaboration] Elliptic Flow for  $\phi$  Mesons and  
176 (Anti)deuterons in Au+Au Collisions at sNN = 200 GeV // *Phys. Rev.*  
177 *Lett.* — 2007. — V. 99. — P. 052301.
- 178 21. *Abelev B.I. et al.* [STAR Collaboration] Centrality dependence of charged  
179 hadron and strange hadron elliptic flow from sNN = 200 GeV Au+Au  
180 collisions // *Phys. Rev. C.* — 2008. — V. 77. — P. 054901.